Isr. J. Earth Sci.; 57: 149–165
DOI: 10.1560/IJES.57.3–4.149

Morphology and dynamics of aeolian mega-ripples in Nahal Kasuy, southern Israel

Hezi Yizhaq,[a] Ori Isenberg,[a] Rimon Wenkart,[b] Haim Tsoar,[b] and Arnon Karnieli[a]
[a]Solar Energy and Environmental Physics, Jacob Blaustein Institutes for Desert Research,
Ben-Gurion University of the Negev, Sede Boker 84490, Israel
[b]The Department of Geography and Environmental Development, Ben-Gurion University of the Negev,
Be'er Sheva 84105, Israel

(Received 3 September 2008; accepted in revised form 2 May 2009)

ABSTRACT

Yizhaq, H., Isenberg, O., Wenkart, R., Tsoar, H., and Karnieli, A. 2008. Morphology and dynamics of aeolian mega-ripples in Nahal Kasuy, southern Israel. Isr. J. Earth Sci. 57: 149–165.

Aeolian sand ripples are a common feature on sandy deserts and beaches. Aeolian ripples often have wavelengths of 10–15 cm and amplitudes of a few millimeters. Mega-ripples are bigger than regular ripples and have a mean wavelength of about 70 cm. They are characterized by a bimodal distribution of coarse and fine particle sizes, which is necessary for their formation. We present here the results of a 1½-year field study at the Nahal Kasuy mega-ripple field, located in the southern Negev Desert. The regular sand ripples superposed on the mega-ripples were formed by weaker winds blowing from different directions. The time evolution of mega-ripples developing from a flat surface was monitored. They grow due to a sand coarsening mechanism. Initially, regular ripples form, which subsequently undergo coarsening by winnowing of the finer particles, thereby producing a coalescence of the regular ripples. The smaller, faster-moving ripples overtake the larger, slower-moving ripples, resulting in increased size and spacing. This state was analyzed by a new technique we developed, using a digital elevation model (DEM) constructed from stereo digital photographs. Data on the wind power (drift potential) during the fieldwork and grain size of samples taken from the mega-ripple crest and trough are presented. The grain-size characteristics demonstrate that only fine particles saltate, while coarse grains creep due to the low wind power at Nahal Kasuy.

1. INTRODUCTION

Aeolian ripples larger and higher than those commonly found in fine sand are known by various names, including ridges (Bagnold, 1941), granule ripples (Sharp, 1963), gravel ripples (Sakamoto-Arnold, 1988), and mega-ripples (Ellwood et al., 1975). Large aeolian sand ripples on Earth have been described in many places, among them the Kelso Dunes and Coachella Valley sands in southern California (Sharp, 1963), as well as those in the Libyan desert (Bagnold, 1941; El-Baz, 1986), the northern Sinai (Tsoar, 1990), Swakopmund, Namibia (Fryberger et al., 1992), northeastern Iceland (Mountney and Russell, 2004), and the northeastern Brazil coast (Yizhaq, 2008). Enormous mega-ripples at an elevation of 4000 m were docu-

E-mail: yiyeh@bgu.ac.il

 0021-2164/08 $4.00

mented in Carachi Pampa, Argentina (Milana, 2009). These mega-ripples, composed of volcanic pebbles, were formed by the action of extremely strong winds (probably the strongest winds known on Earth, ~400 km/h). Their wavelengths are up to 18 m and their heights are about 1.5 m (Milana, 2009).

There is a correlation between the mega-ripple wavelength λ and height (which is given as a ripple index, $RI = \lambda/h$, of approximately 15), as well as between the wavelength and maximum particle size (see figs. 3 and 4 in Williams et al., 2002). According to Bagnold (1941), it may take decades or centuries to form huge mega-ripples, with their dimensions varying as the square root of age. However, from his studies of the Kelso Dunes, Sharp (1963) suggests that with a large enough supply of coarse grains, it might take only weeks for well-defined granule ripples to form. It was also observed that during a severe windstorm in the southern San Joaquin Valley in California, mega-ripples formed on a timescale of hours or days (Sakamoto-Arnold, 1988). For large mega-ripple bedforms to develop, a bimodal distribution of particle sizes seems to be required, as was shown by Sharp (1963), who found that coarse grains compose 50–80% of the crest material and less than 10–20% of the trough.

In wind tunnel experiments, "proto" granule ripples were found to drift about 1 cm downwind every 5 min (Fryberger et al., 1992). Recent field experiments carried out in Morocco indicate that the initial wavelength, as well as crest height, increases with wind speed (Murray, 2005). In addition, mega-ripple wavelength grows via a coarsening process similar to that occurring in normal ripples, in which ripple wavelength increases due to coalescence of smaller ripples (Murray, 2005). Table 1 summarizes the main characteristics of normal ripples and mega-ripples.

Large ripple-like bedforms have been observed in numerous locations on Earth (Edgett, 2001; Williams et al., 2002; Greeley et al., 2002; Wilson et al., 2003; Yizhaq, 2005). Interestingly, aeolian processes are also important for understanding the geology of Mars (Rubin, 2006). Images from the Mars Global Surveyor clearly portray dust storms, dust devil traces, dunes, and mega-ripples. Various applications of sand ripple studies on Earth and Mars were recently reviewed by Rubin (2006).

In his seminal book, Bagnold (1941) was the first to explain the formation of mega-ripples. He pointed out that the essential difference between normal ripples and mega-ripples lies in the relative magnitudes of wind strength and grain-size distribution. In the case of mega-ripples, the wind is not strong enough to cause coarse particles to saltate. Bagnold (1941) specifies the following conditions for mega-ripple formation: (i) availability of sufficient coarse grains with a diameter 3–7 times larger than the mean diameter of the grains in saltation; (ii) a constant supply of fine sand in saltation to sustain forward motion of reptating, creeping, or slipping of coarse grains; and (iii) a wind velocity below the threshold that would drive coarse grains from the mega-ripple crest. His theory specifies that mega-ripples will grow indefinitely as long as the supply of fine particles is maintained.

Bagnold also describes a strong-wind situation in which coarse grains can be driven into saltation, with mega-ripples breaking down into normal ripples. Sharp (1963), in his field studies of the Kelso Dunes and Coachella Valley, California, confirmed Bagnold's ideas of mega-ripple formation but indicated that the principle of characteristic grain path is probably not applicable to the wavelength of mega-ripples. Sharp suggested that most of the considerations pertaining to normal ripples, including impact slope, shadow slope, height, and mean impact angle of saltating grains, can be applied to mega-ripples. Sharp showed that a concentration of larger grains capable of covering at least 50% of the crest surface is required for producing well-developed mega-ripples. He also noted that mega-ripples form and move slowly and have considerable longevity compared to normal sand ripples.

Table 1
Main features of normal aeolian ripples and mega-ripples

	Normal ripples	Mega-ripples
Wavelength (λ)	Up to 30 cm	30 cm–20 m
Ripple index	>15 (Sharp, 1963)	<15 (Sharp, 1963)
Timescale	Minutes (Anderson, 1990)	Days (Sakamoto-Arnold, 1988) and years (Bagnold, 1941)
Sorting	Unimodal distribution of grain sizes (typically 0.06 to 0.5 mm in diameter)	Bimodal distribution of grain sizes with coarse grains 1–4 mm in diameter
Basic Processes	Saltation and reptation of fine grains	Saltation of fine grains and creep of coarse grains.

In a carefully designed experiment in a 30-m-long wind tunnel, Walker (1981) showed that normal ripple spacing and height increase with increasing grain diameter and with sorting. The observed segregation parallels that of similarly sized sediments during natural aeolian transport and deposition. Walker argued that although flow separation does not occur over the crest of aeolian mega-ripples, an analogous situation develops. When the ripple grows high enough, it casts a "shadow" that shelters the ripple's lee slope from saltation bombardment. Walker considered that this shadow zone may be important for mega-ripple formation. Based upon experiments with poorly sorted sands, he suggests that at a given value of wind-shear stress the increasing concentration of coarse grains at the crest allows the ripple to continue growing higher. He bases this conclusion on the fact that coarse grains are harder to dislodge by saltating fine grains and they are also more resistant to direct wind shear.

Tsoar (1990) studied the surface grain-size distributions of the crests and troughs of mega-ripples with wavelengths of 25 cm and longer that formed on the plinth of a desert seif dune in the northern Sinai. He used a unique sampling technique in which the surface of the ripple crest and trough were sprayed separately with an adhesive. Following treatment with solvent to dissolve the glue, dispersion of the particles with a high-intensity sonic processor, washing, and drying, the samples were analyzed using standard sieves. Grain size of the surface layer of the mega-ripple particles was shown to be trimodal, with one prominent coarse-grain mode and two small fine-grain modes. The frequency of coarse grains decreases in the underlying two below-surface laminae and almost disappears at a depth of several centimeters.

In contrast to Williams et al. (2002), who studied large mega-ripples at Edwards Air Force Base in southern California and at Great Sand Dunes National Monument in southern Colorado, Tsoar (1990) found that the wavelengths of mega-ripples were not significantly correlated with the mean crest- or surface-grain size or with the mean size of grains in the entire mega-ripple. This difference may be explained by the fact that Tsoar (1990) sampled mega-ripples with wavelengths between 25 and 50 cm, which can be considered nonrepresentative, small mega-ripples. Moreover, he examined correlations with respect to mean grain size alone, but a correlation might have been found had he examined wavelength vs. maximum grain size, as was observed by Williams et al. (2002). In addition, Tsoar (1990) found no continuity between increasing mean grain size and wavelength of normal ripples and mega-ripples. The question of continuity was also addressed by Ellwood et al. (1975, fig. 7c), who analyzed 120 samples and found no discontinuity in the plot of wavelength against the coarse twenty-percentile grain size (P_{20}) for ripples and mega-ripples. They, therefore, concluded that ripples and mega-ripples were formed by the same mechanism. This disagreement between Tsoar (1990) and Ellwood et al. (1975) may derive from the large number of samples taken by Ellwood, which covered many more wavelengths.

In recent work at the White Sands National Monument, New Mexico, USA, Jerolmack et al. (2006) measured the sand flux of coarse-grained ripples with wavelengths between 0.5–1 m and heights of 10 mm. They found that the small particles (0.1 to 1 mm) were transported by saltation and the coarse grains (1 to 3 mm) by surface creep. They observed a clear spatial segregation between the two populations of grains. The coarse grains were concentrated on the crest, while the trough contained few coarse grains. This is the first field experiment that supports Bagnold and Elwood's hypotheses of mega-ripple formation that coarse grains are transported solely by creep. However, the relatively small, 10-mm-high coarse ripples they studied should be classified as atypical, shallow mega-ripples.

Although the dimensions and compositions of mega-ripples have been documented in the field, the evolution of mega-ripple formation has not yet been studied in fieldwork or by wind tunnel experiments, nor is there yet a convincing mathematical model of mega-ripple development. The relative role of the bimodal grain-size distribution and wind strength on mega-ripple formation is also unknown. In this study we shed light on these open questions.

2. RESEARCH AREA AND METHODS

2.1. Research area

Our field experiment was carried out on the Nahal (wadi) Kasuy sand dunes in the southern Negev (Fig. 1), which cover an area of 15 km^2 (Ginat, 1991). The aeolian sand in this area is composed of 60% calcite and 35% quartz. It drifts into Nahal Kasuy from the Uvda Valley by SW storm winds and piles up in the wadi bed (Fig. 1). The annual precipitation rate here is about 37 mm, and shrubs of *Haloxylon persicum* sparsely cover the wadi bed.

The mega-ripple field is located in the middle of the wadi, where coarse grains abound. The mega-ripple

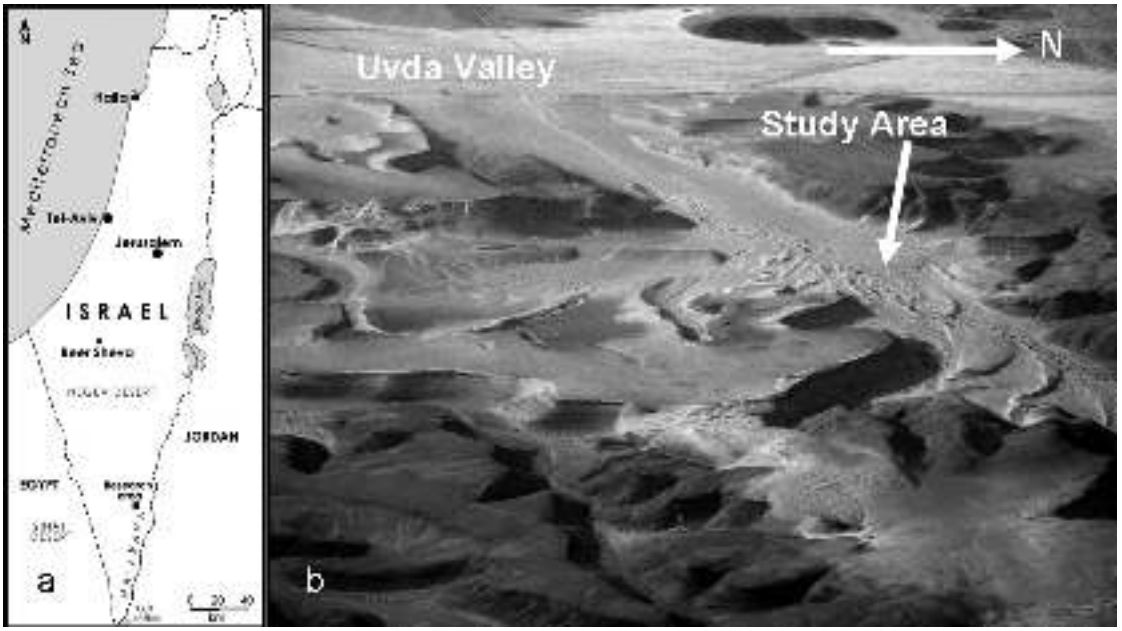

Fig. 1. (a) The research area (indicated by a black square) is located in the southern Negev, 46 km north of the Gulf of Elat. (b) An aerial photo of Nahal Kasuy. The mega-ripples are found in the middle of the wadi (indicated by the white arrow; their location is 29°59′14″N; 34°59′25″E, 430 m above mean sea level).

Fig. 2. Mega-ripples at the field study site with an average wavelength of 70 cm. Normal ripples can be seen between the mega-ripples. The wind direction is from left to right. The photograph was taken on 22 Jun 2008.

mean wavelength is about 70 cm, with a mean height of about 7 cm ($RI \sim 10$). Smaller ripples are superimposed on the mega-ripples and reflect the last wind direction (Fig. 2). Kasuy mega-ripples are quite small when compared to those in other parts of the world. In a nearby field of mega-ripples in Wadi Rum, Jordan, the mega-ripple height is about 0.4 m and the wavelength about 3 m. Because of their relatively small size, Kasuy's mega-ripples are expected to be more sensitive to storms that form and modify them.

To study mega-ripple evolution we flattened three plots and hand-mixed the grains to achieve a uniform distribution of coarse and fine grains. The plot sizes and the dates of flattening are given in Table 2 (see also the map in Fig. 3). The fourth (D) and the fifth (E) plots were not flattened but were marked to track changes of the large and medium-size mega-ripples.

2.2. Wind speed measurements

Wind speed and direction measurements at a height of 3.3 m were carried out by two anemometer recorders that were placed at the eastern edge of the mega-ripple field. The wind speed was used to calculate the drift potential (DP) and the resultant drift potential (RDP) (Fryberger, 1979). Theoretical and empirical studies show that the potential sand volume transported by the wind through a 1-m-wide cross section per unit time is proportional to DP (Fryberger, 1979). DP is calculated from

$$\mathrm{DP} = \langle u^2 (u - u_1) \rangle \qquad (1)$$

where u is the wind speed (in knots; 1 knot = 0.514 m/s) measured at a height of 10 m and averaged over time; and u_1 is the minimal threshold velocity (= 12 knots) necessary for sand transport (Fryberger, 1979). The direction of RDP is referred to as resultant drift direction (RDD), which expresses the net trend of sand drift, namely, the direction in which sand would drift under the influence of winds blowing from various directions. It is calculated by vector summation of the DP

Table 2
Plot description

Plot	Date of beginning and characteristics	Size
A	Flattened in January 2008 and marked with iron rods serving as Ground Control Points	5 × 5 m
B	Flattened in January 2007	5.5 × 5.5 m
C	Flattened in November 2006	4 × 4 m
D	March 2008, large-size mega-ripples	5 × 5 m
E	June 2008, medium-size mega-ripples	5 × 3 m

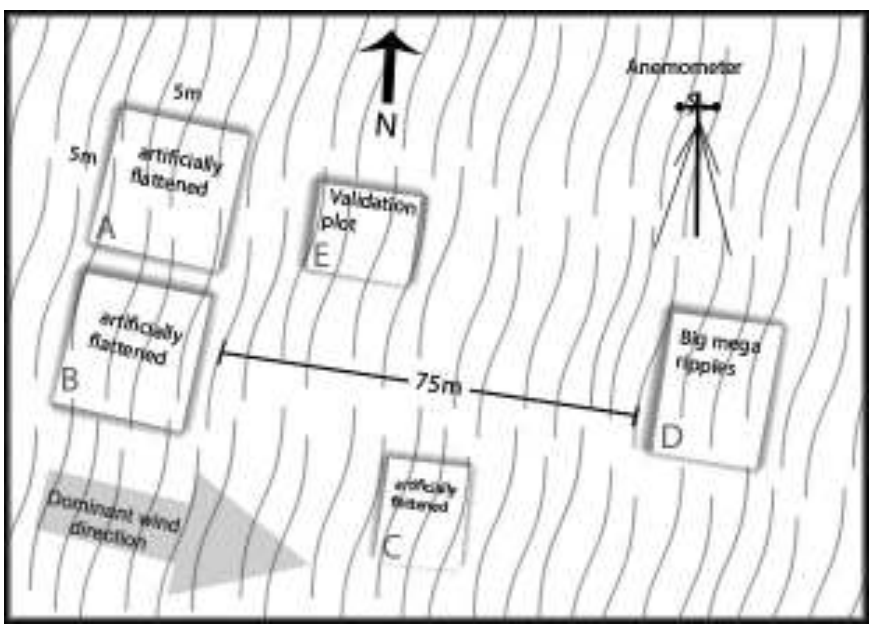

Fig. 3. Schematic map of the plots at Nahal Kasuy. Plots A, B, and C were artificially flattened, and plots D and E were used to track mega-ripple spatial dynamics.

from the different directions. The ratio of RDP to DP (RDP/DP) is an index of the directional variability of the wind (RDP/DP = 1 stands for unidirectional wind whereas RDP/DP = 0 characterizes multidirectional winds, which vectorally cancel each other). DP is the potential sand drift, whereas the actual sand drift potential further depends on the mean grain diameter, the degree of surface roughness, the amount of vegetation cover, and sand moisture. For the calculation of DP, the wind speed at a height of 10 m needs to be computed. This can be done by using the Karman–Prandtl velocity distribution equation (Wiggs, 1997),

$$\frac{u}{u_*} = \frac{1}{\kappa}\ln\frac{z}{z_0} \tag{2}$$

where κ is von Karman's constant (= 0.4), u is the wind speed at height z, u_* is the shear velocity, and z_0 is the aerodynamic roughness. According to Bagnold (1941) $z_0 \approx d/30$, where d is the mean grain diameter assuming well-sorted particles with homogeneous surfaces. z_0 also depends on the larger particles and their spacing (Wiggs, 1997) and can be as large as $d/8$. Using wind speed measurements taken at a height of 3.3 m ($u_{3.3}$), eq 2, and the estimated value of z_0, the wind speed at the standard height of 10 m (u_{10}) can be calculated (Lee et al., 1994) from

$$u_{10} = \frac{u_{3.3}\ln(10/z_0)}{\ln(3.3/z_0)} \tag{3}$$

To obtain DP, we used $z_0 = d/25$ with d = 0.25 mm, which is the mean grain diameter usually used for such calculations. For these values the correction factor $\ln(10/z_0)/\ln(3.3/z_0)$ is 1.087. We also compare our results with wind measurements conducted at the meteorological station located at Uvda airport (30ºN, 34.883ºE).

2.3. Grain-size analysis and its importance

Sixty samples of sand were retrieved from the field study by using a tunafish can (diameter 84 mm, height 35 mm), which was pressed into the cross section of the mega-ripple under study (Plot D) (λ = 0.75 m). Samples were obtained from the trough, windward face, crest, and leeward slope, as well as from incipient mega-ripples (λ = 0.15 m) and normal ripples. The samples were scooped out of the can with a flat scraper. We also took 10 samples from nearby normal sand ripples for comparison with those of the mega-ripples. All the samples were taken on the same day (5 February 2008). The average weight of the samples was 310 g (with values ranging between 282 and 336 g). The samples were divided into 2 by a splitter. The grain-size distribution was obtained by means of standard sieves suspended on a shaker. The aperture of each sieve was greater by 1/4 ϕ than the one above ($\phi = -\log_2 d$).

The grain-size analysis also contributes to the understanding of mega-ripple formation by enabling an estimation of the threshold velocity needed to dislodge the coarse grains on the dune crest. According to Bagnold (1941), the threshold shear velocity is given by:

$$u_{*cr} = A\sqrt{\frac{\rho_s - \rho}{\rho}gd} \tag{4}$$

where ρ_s is the grain density, ρ is the air density, g is the acceleration of gravity, and d is the grain diameter, with A being a coefficient ($A \approx 0.1$) that depends on the grain Reynolds number (Wiggs, 1997). Using eqs 2 and 3 gives the threshold velocity u_t at height z,

$$u_t = \frac{1}{\kappa}A\left(\frac{(\rho_s - \rho)gd}{\rho}\right)^{1/2}\ln(z/z_0) \tag{5}$$

Figure 4 shows the threshold velocity at 3.3 m as a function of the grain diameter for different choices of surface roughness, z_0. As z_0 increases, threshold velocity decreases. However, the differences are quite small for grains with d < 1mm.

Equation 5 is an estimation of the threshold velocity, as it is only correct for a unimodal distribution of identical grains. This is not the case for the mega-ripple crest. For mixed size grains, the critical shear velocity can be much smaller for coarse grains on a bed composed primarily of fine particles (Fenton

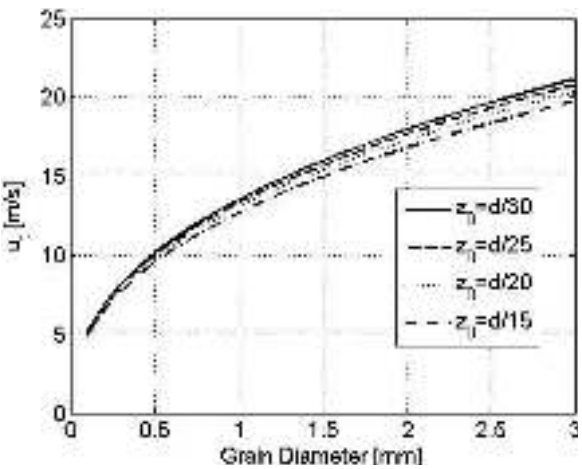

Fig. 4. Threshold velocities at height 3.3 m according to eq 5 as a function of the grain diameter for different choices of z_0. Parameter values: A = 0.1, κ = 0.4, ρ_s = 2710 kg/m^3 (calcite), ρ = 1.2 kg/m^3, g = 9.8 m/s^2 (Defoe and Compton, 1925).

and Abbott, 1977; Raudkivi and Ettema, 1982; Jerolmack et al., 2006), as they are more exposed to wind and because the angle of repose is smaller for a coarse grain resting upon fine grains (Wiberg and Smith, 1987). In addition, we assume that the grain entrainment takes place via the drag and lift forces of the moving air (a mechanism that works through a fluid threshold). The fluid threshold velocity is the upper limit for grain entrainment because the impact of the saltating grains can drive other grains into saltation, an impact-driven threshold that is about 0.8 of the fluid threshold (Anderson and Haff, 1988). Figure 4 gives important information about the wind speed necessary for coarse-grain saltation, which can remove the mega-ripple armoring and break it into small ripples, as suggested by Elwood et al. (1975).

2.4. Photogrammetry

To produce digital photographs, we used RGB (red-green-blue) images from a digital Nikon D80 camera with a Sigma 10–20-mm lens. Processing took place with Erdas Imagine version 9.1 and its Leica Photogrammetry Software (LPS) extension. Use of the small focal-length lens of 10 mm, which corresponds to a 94.5º field of view results in reducing the number of photographs needed to cover the plots. Altogether 10% were cropped from the edges of every image to reduce lens distortion. To avoid interfering with plot dynamics, the imaging and the ground control point (GCP) markings had to be made from outside. The camera was mounted on a special rail (5 m long) that was fixed on two tripods at its sides. The camera could be moved along the rail by two cords attached to the camera. We used a remote control cable to operate the camera.

Initially the GCPs were used for geometrical rectification. In principle, GCPs could be placed outside the plots to derive DEM with photogrammetry. However, we found out for our work that the GCPs must be placed throughout the plots in order to acquire an accurate DEM. The first method was used for plot A, and involved iron rods, 0.6 mm in diameter and 12 cm in height above the surface, which were installed in specific, well-defined points. Those rods give the *x,y*, as well as the *z* (height) coordinates. Our decision to use long rods instead of flat GCP panels resulted from the constantly changing surface levels, which led to GCP panels being covered by sand.

The second method, which was used in the other plots (B, C, D, and E), involved marking holes on the surface by using a giant "comb". The comb (5 m long) pinches the surface and leaves marks on the sand at intervals of 15 cm; these are used as GCPs .We ensured that the marks are always in the same locations by placing the combs in the same starting points that were marked by iron pegs. The locations of the holes give only the *x,y* coordinates, without *z* values. We photographed the plots every three weeks.

2.4.1. Processing and analysis

Image analysis was carried out with LPS Project Manager. To reduce the need for a large number of GCPs for each plot, LPS Project Manager uses the self-calibrating bundle block adjustment method. With this approach, the internal geometry of each image and the relationship between overlapping images is determined with a small number of GCPs.

The only manual process needed for implementing this approach is geometric rectification. After carrying this out, the program automatically extracts all the data needed for the "Automatic Terrain Extraction" feature embedded in the LPS. The main product we used in this study was the Digital Terrain Model (DTM) in DEM format. The DEM provides the two most important parameters in ripple measurement: wavelength and ripple height. By measuring these parameters together with continuous wind measurements, we can track temporal topographic changes.

The quality of the DEM depends on many factors. We found that the best results came out when images were taken in the late afternoon, when contrast is at a maximum. By selecting the camera AutoMode option, aperture and shutter speed were chosen automatically; no significant deviations in color or hue were noticed among the pictures.

Figure 5 shows two layers that describe one of the plots at a given time. The lower layer is the DEM. The

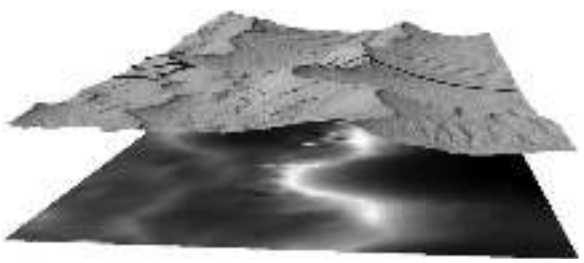

Fig. 5. Two layers that describe one of the plots (3.8 × 2.4 m). The lower layer is the DEM. White describes the higher elevation places and the dark part, the lower places. The upper layer is the orthophoto of the plot representing it in three dimensions based on the DEM data below it (vertical exaggeration ×2). The orthophoto shows two large mega-ripple crests with small ripples at the trough between them.

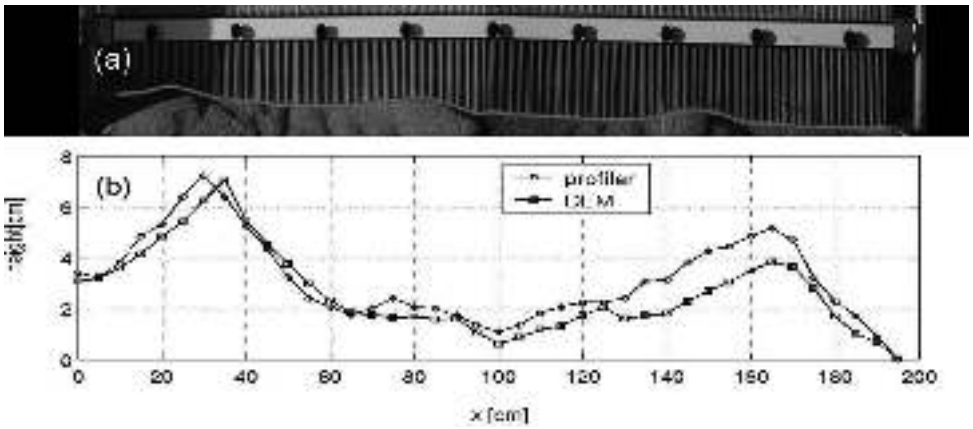

Fig. 6. (a) The profiler used to measure mega-ripple profiles in plot E. (b) The measured and DEM profiles are shown together. (The wind direction is from left to right.) The agreement between the two is highly satisfactory.

upper layer is the orthophoto of the plot, representing it in three dimensions based on the DEM data below it (vertical exaggeration ×2).

2.4.2. Validation

In order to validate the correctness of the measurement scales, we performed the following test. We used a mechanical profiler, working on the principle of a "nail board" that can capture the structure of the ripples measured with the DEM method. This procedure helps to compare accurately the digital and true ripple profiles. Figure 6 shows two profile curves of mega-ripples in plot E, one done with the profiler and the second with the photogrammetry technique. To quantify the similarity between the two curves we use the similarity S index (Kuragano and Yamaguchi, 2006) as given by

$$S = \frac{h_1 \cdot h_2}{|h_1||h_2|} \tag{6}$$

where h_1 and h_2 are the height vectors, i.e., their components are the height of the ripples at equal x intervals, $h_1 \cdot h_2$ is the scalar product between the two height vectors, and $|h_1|$ and $|h_2|$ are the lengths of the vectors h_1 and h_2, respectively. For two identical curves $S = 1$. For the two profiles shown in Fig. 6, $S = 0.98$, indicating the high accuracy of the photogrammetry method.

3. RESULTS

3.1. Winds at Nahal Kasuy

3.1.1. Drift potential

Table 3 summarizes the monthly wind drift potential

Table 3
Wind power data for Nahal Kasuy, 2007. The total drift potential (DP) that year was 48.67, indicating a low wind-power environment according to Fryberger's classification (1979)

Month	DP	RDP	RDP/DP	RDD	T (%)
January	9.05	6.75	0.75	271	9.68
February	9.65	7.91	0.82	262	11.2
March	8.37	6.93	0.83	273	8.06
April[1]	11.1	5.53	0.50	1.99	12.1
May[1]	5.38	3.27	0.61	236	10.8
June	1.60	1.46	0.92	316	5.50
July	1.38	1.25	0.91	317	5.29
August	0.47	0.42	0.90	325	3.00
September	0.68	0.64	0.94	330	3.26
October	0.08	0.03	0.44	272	0.63
November	0.34	0.18	0.54	198	1.50
December	0.63	0.59	0.95	268	1.64

[1]Due to problems with our anemometer, data from the nearby meteorological station of Uvda airport were used for these two months.

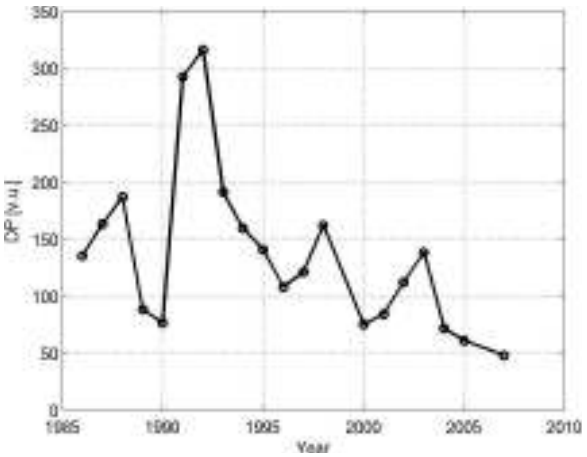

Fig. 7. Drift potential (DP in v.u.) calculated from wind data of Uvda airport (30ºN, 34.883ºE) for the years 1986–2007. DP values show great annual variability. In 2007, DP was the lowest since 1986 and less than one-sixth of that in 1992. The mean DP for this period is 136 with a standard deviation of 71.

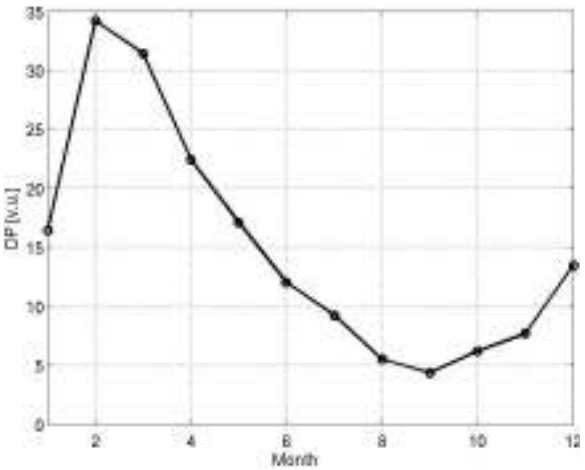

Fig. 8. Monthly average drift potential (DP in v.u.) calculated from wind data at the Uvda airport (30ºN, 34.883ºE) for the years 1983–1993. During the winter the DP values are higher and February is the windiest month for this period.

(DP) parameters for 2007. The total DP (in vector units, v.u.) for 2007 was 48.67, which is quite low. This value is very similar to that calculated for the nearby Uvda airport (DP = 47.43) and was the lowest yearly DP measured since 1986 (Fig. 7). The considerable annual variability in DP values is due to storm events that, although short, can significantly change the annual average. For example, the DP in 1992 was more than six times that of 2007. The value of DP depends on the temporal resolution of the measurements. As expected from the third-power relationship of DP with the wind speed, the finer the resolution the larger the DP, and the correlation with actual sand transport is better. We used measurements at intervals of 10 min for the calculation of DP. Table 4 presents the wind statistics for the first ten months of 2008.

With regard to Fig. 7, it is important to note that the Pinatubu volcano eruption in the Philippines occurred on 15 June 1991, and the winter of 1992 in Israel was characterized by an overabundance of precipitation and snow. 1992 was also an El Niño year, usually correlated with high precipitation rates in Israel. Figure 8 shows the average monthly DP values for the years 1983–1993 at the Uvda airport. The highest values of DP occurred during the winter. These unique conditions may explain the unusually high DP (136) for Uvda Valley in 1992, which is far above the mean value for this locale.

3.1.2 Storm characteristics

Due to the cubic dependence of DP on wind speed, high wind storms contribute significantly to DP.

Table 4
Wind power data for the first ten months of 2008 at Nahal Kasuy. January 2008 was the month with the highest DP value during our entire period of measurements

Month	DP	RDP	RDP/DP	RDD	T (%)
January	12.8	12.1	0.95	256	8.67
February	5.62	5.34	0.95	272	6.15
March	4.2	1.74	0.42	222	7.40
April	4.3	0.64	0.15	245	7.89
May	4.94	4.33	0.88	266	5.78
June	4.38	4.14	0.95	296	8.17
July	1.35	1.30	0.96	333	4.30
August	0.75	0.68	0.91	319	3.30
September	0.43	0.39	0.9	305	2.60
October	0.21	0.11	0.51	280	1.20

Storms in Nahal Kasuy occur during the winter and spring, while summer and fall are of very low wind power. Figure 9 shows the wind speed and wind direction of three storms that occurred during the winter and spring of 2007.

All three storms have their highest wind speeds in the afternoon; their duration is approximately 10 h, in agreement with the general pattern in Israel (Goldreich, 1998). The strongest storm measured was on 8 May 2008 (Fig. 10).

Most of the storms occurred during daylight hours, except for the 2-day-long storm of 30 January 2008, where strong winds also blew during the night. This long-duration storm had a significant impact on the morphology of the field study due to the massive sand transport, as shown below.

3.2. Grain-size analysis

Table 5 presents the average moments at the six sampling points and the median (where 50% of grains are coarser). The analysis was performed by GRADISTAT software (Blott and Pye, 2001). The four moments determined are the mean or average particle size, sorting, skewness, and kurtosis.

These results show clearly that the coarser grains are concentrated at the mega-ripple crest (mean 0.35 mm), and the finer grains are found in the trough (mean 0.2 mm). The coarse mode for the crest sample is d = 780 μm, whereas that of the incipient mega-ripples is d = 550 μm. The fine mode at the trough is d = 116 μm. These results indicate that as the size of the coarse particles covering the crest increases, so does the mega-ripple wavelength increase. This is in agreement with former studies (Walker, 1981; Tsoar, 1990).

The sorting (standard deviation) is related to the range of grain size. Hence, since the sample is taken to a depth of 35 mm, it is largest (406 μm) at the mega-ripple crest since it contains the coarsest grains at the upper layer and the fine particles beneath. The samples taken from the incipient mega-ripples and from the mega-ripple crests are poorly sorted (371 and 219 μm, respectively). This result supports Walker's (1981) conclusion that ripple wavelength also depends on sorting and can increase as sorting becomes poorer, i.e., the difference between the coarsest and finer particles increases. The normal ripple samples are well sorted and show a unimodal distribution (mean 160 μm).

Skewness is one of the more sensitive parameters for characterizing sediments. According to Table 1, all the samples are symmetrically skewed except for the crest sample, which is finely skewed, and the normal ripple sample, which is very finely skewed (Blott and Pye, 2001). At the lee slope, the skewness is negative but still in a range where it is considered symmetrical. Kurtosis values of all the samples were above one, which indicates a leptokurtic distribution. The highest values were found in the trough samples, where the mean size was smallest, thus the concentration around the mean was the largest. The grain-size distribution (in μm) of the 10 samples from the different parts of the mega-ripples is shown in Fig. 11.

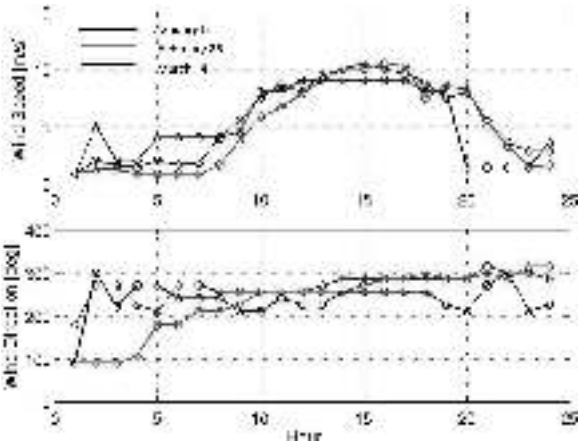

Fig. 9. Three storms at Nahal Kasuy during 2007. The wind speed increases between 10:00–20:00. The highest wind speed during these storms was about 11 m/s, which is below the threshold velocity needed for saltation of coarse particles (14 m/s for a grain with a diameter of 1 mm).

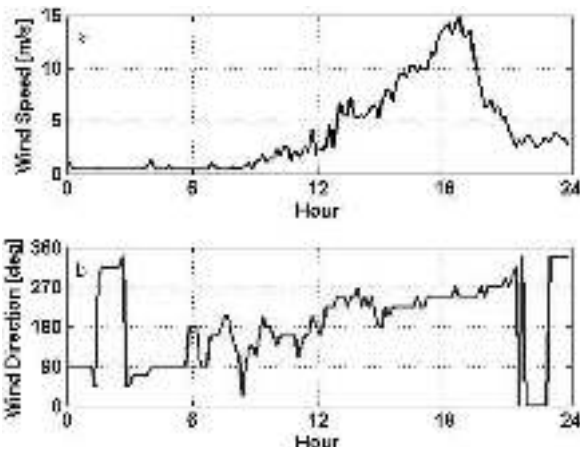

Fig. 10. Recording of 8 May 2008 storm at 10-min intervals. This westerly storm had a maximum speed of 15 m/s, the highest wind speed measured during this study.

Table 5
The average (ϕ) moments at the six sampling points at Nahal Kasyu (mega-ripples in plot D, incipient mega-ripples, and normal ripples taken on 5 February 2008), median (D_{50}), and the sample type as calculated by GRADISTAT (Blott and Pye, 2001). The last row in the table shows the moments for the crest samples taken from large mega-ripples at Wadi Rum in southern Jordan

Sampling location	$(\bar{x}_\phi)$ mean	σ_ϕ sorting	Sk_ϕ skewness	Kg_ϕ kurtosis	Median–D_{50} (μm)	Sample type
Windward face	2.19	0.98	0.10	6.30	200	trimodal, moderately sorted
Crest	1.51	1.30	0.46	3.08	369	trimodal, poorly sorted
Lee slope	2.04	1.06	–0.03	4.48	218	polymodal, poorly sorted
Trough	2.31	0.84	0.26	8.29	194	bimodal, moderately sorted
Incipient mega-ripples (λ = 15 cm)	1.91	1.08	0.01	0.66	285	polymodal, poorly sorted
Normal ripples (λ = 8 cm)	2.65	0.55	1.60	17.94	158	unimodal, well sorted
Wadi Rum mega-ripples, crest (λ = 217 cm)	0.52	1.18	0.24	2.08	672	bimodal, poorly sorted

Mega-ripple crest distribution is trimodal (one coarse-grained mode and two small fine-grained modes) where there is an abundance of coarse particles. However, samples taken from the normal ripples show typical unimodal distribution with a dominant fine fraction mode. The coarse mode for the crest sample is d = 780 μm and fine mode at the trough is d = 116 μm, whereas the coarse mode of the incipient mega-ripples is d = 550 μm. Figure 11 also includes grain analysis curves (dashed lines) of samples taken from mega-ripples at Wadi Rum in southern Jordan. The analysis was done by using the same technique as used in Nahal Kasuy. These mega-ripples are quite large with a mean wavelength of 2.17 m. The overall distribution between the small mega-ripples at Nahal Kasuy and large mega-ripples at Wadi Rum is the same, but there is a significant shift to the coarser grains for the latter (the shift is both for the coarse and fine modes). The coarse

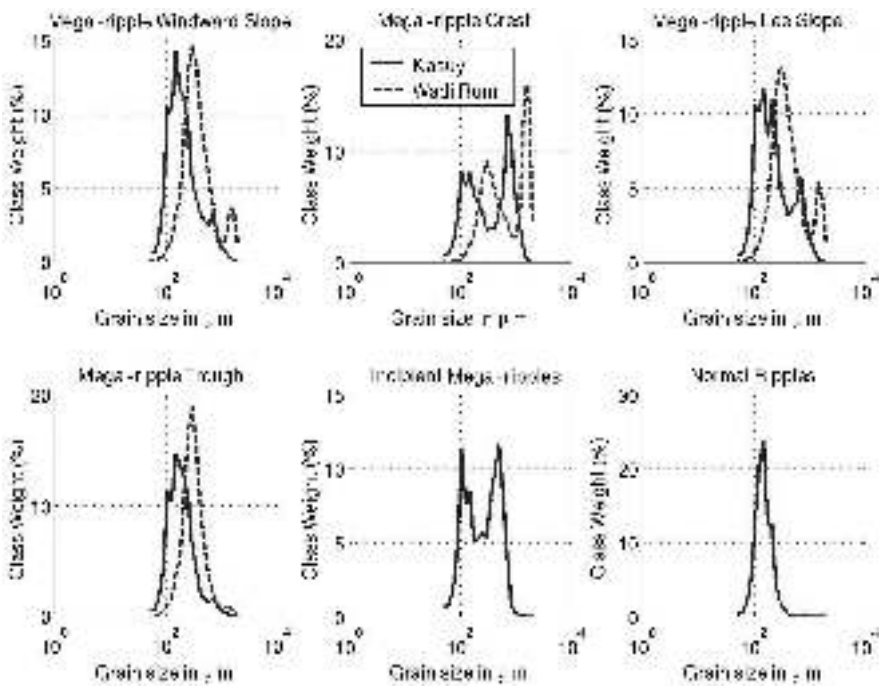

Fig. 11. Grain size distributions of the average 10 samples taken from mega-ripple windward faces, crests, lee slopes, troughs, incipient mega-ripple, and normal ripples. The coarser mode at the crest is d = 780 μm, whereas the finer mode of the trough sample is d = 115.5 μm. The average wavelength of Wadi Rum mega-ripples is 2.17 m, considerably larger than the Nahal Kasuy mega-ripples.

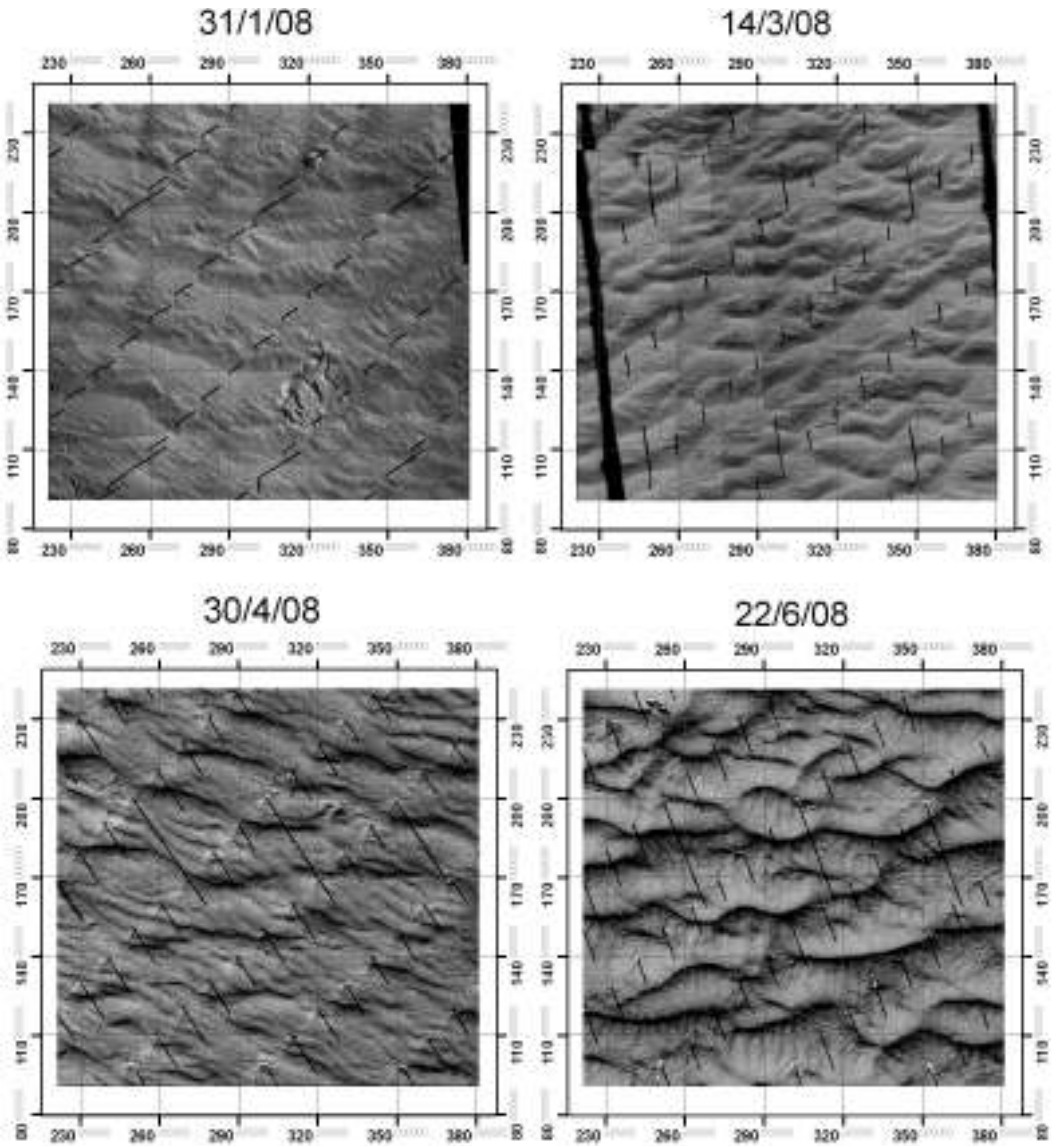

Fig. 12. Ripple evolution from a flat bed (plot A) at four different times, as indicated in the titles, and of a square portion of 1.6 × 1.6 m. The plot was flattened and marked with iron rods in December 2007 (their shadows are seen as black lines). The upward direction in the figure points to an azimuth of 295º. The small ripples coarsened during this period and their wavelength increased to 30 cm. See text for details.

mode for the crest sample at Wadi Rum is $d = 1850$ μm compared to $d = 780$ μm at Nahal Kasuy. These results indicate that the larger the coarse particles that cover the crest, the larger the mega-ripple wavelength, in agreement with former studies.

3.3. Topography field analysis of mega-ripples

3.3.1. Ripple evolution from a flat bed

The evolution of plot A during the first six months is shown in Fig. 12. At the initial stage the ripples are quite small, with discontinuous crests that responded quickly to the prevailing winds. Their direction of movement during the first three months is inconsistent. Afterwards their wavelengths and heights increase. After almost seven months their wavelength is about 30 cm and their crests are more continuous. Normal ripples perpendicular to the larger ripples can be seen at the troughs. Between 30/4 and 22/6 the ripple direction had changed from 308º to 295º, as they responded to the westerly May 8 storm (see Fig. 9). During this period the small

ripples (λ = 5 cm), which are seen on April 30, disappeared as the larger ripples became more prominent.

Figure 13 shows the wind speed above 6 m/s and direction distributions for February, March, and April 2008. In 53% of these measurements, wind direction was in the range 240°–300°. This can explain the observed ripple direction, which should be perpendicular to the prevailing winds. Since DP in the first months of 2008 was quite low, ripple evolution was slow, and after six months the wavelength was of the order of 30 cm. Thus, in such a low wind energy environment, it may take one or two years for mega-ripple formation to proceed. Figure 14 shows a profile of three mega-ripples carried out on 27 March 2008,

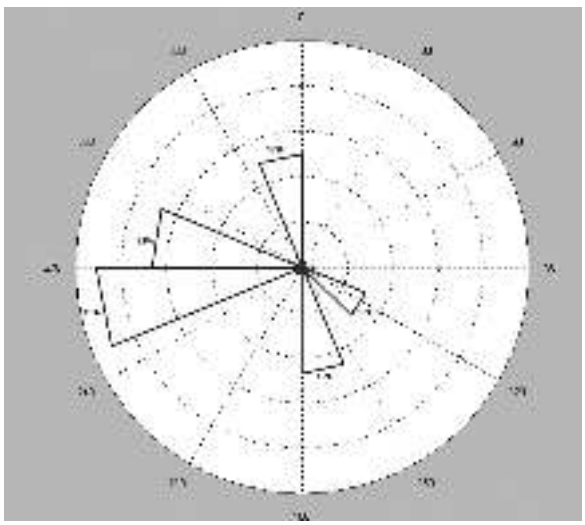

Fig. 13. Wind rose for speeds above 6 m/s, showing wind direction distribution between February and April 2008 (5.7% of all the measurements).

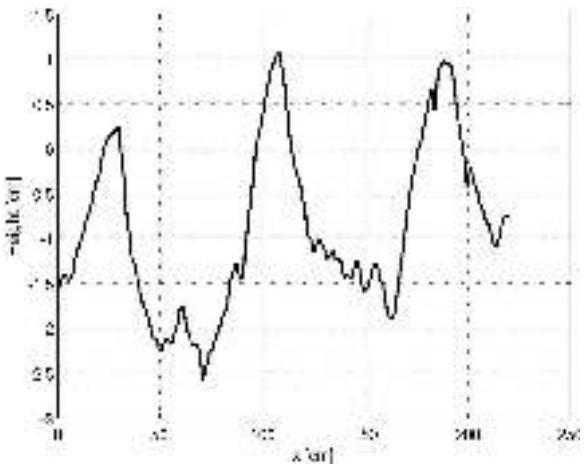

Fig. 14. Mega-ripple profile produced from a DEM of plot B on 27 March 2008, which was flattened in January 2007 (the wind direction is from left to right). The wavelength is 73.3 cm and the mean height 2.61 cm. Note that the profiles are asymmetric and show a steeper lee slope. Small ripples can be seen in the trough between the mega-ripples.

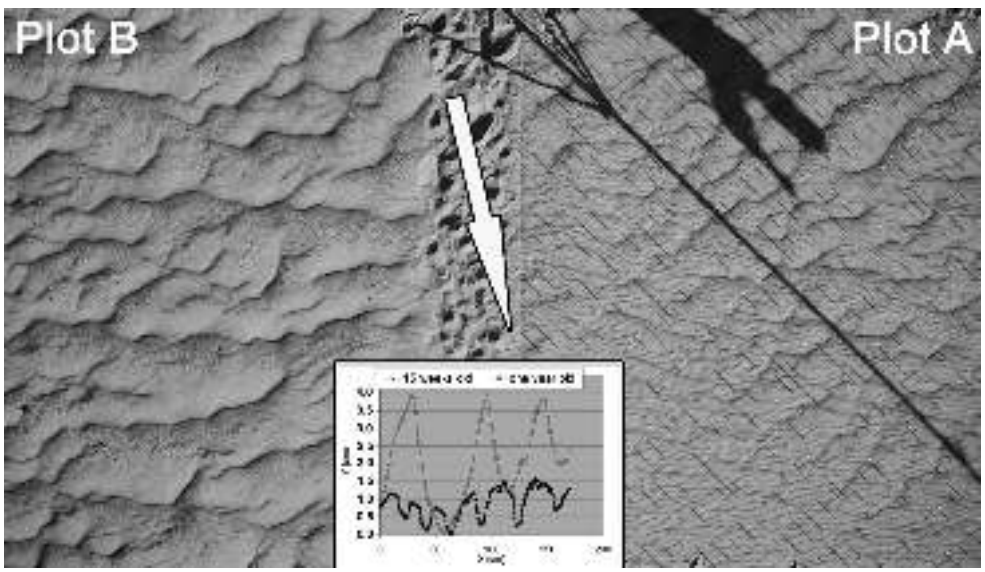

Fig. 15. Plots A (*right*) and B (*left*) photographed simultaneously. The difference between the plots is that plot B was flattened one year earlier than plot A. The inset shows typical ripple cross sections. The average wavelength in A is 28.4 cm and in plot B is 56.7 cm.

which developed in plot B, which had been flattened in January 2007.

Figure 15 shows the two adjacent plots (A and B) that have the same initial grain sizes. The difference between the two plots is that plot B was flattened one year before plot A, thus the mega-ripples had more time to develop. The average wavelength in A is 28.4 cm and the average height is 0.8 cm, whereas for plot B the average wavelength is 56.7 cm and the average height is 3.4 cm. Plot B can be regarded as an onward stage in the evolution of the "young" mega-ripples in plot A.

3.3.2. Mega-ripple dynamics under storm events

The storm of 8 May 2008, shown in Fig. 9, was accompanied by very high speed winds (up to 15 m/s). We documented its effects on the different plots. Figure 16 shows three plots before and after the storm. They

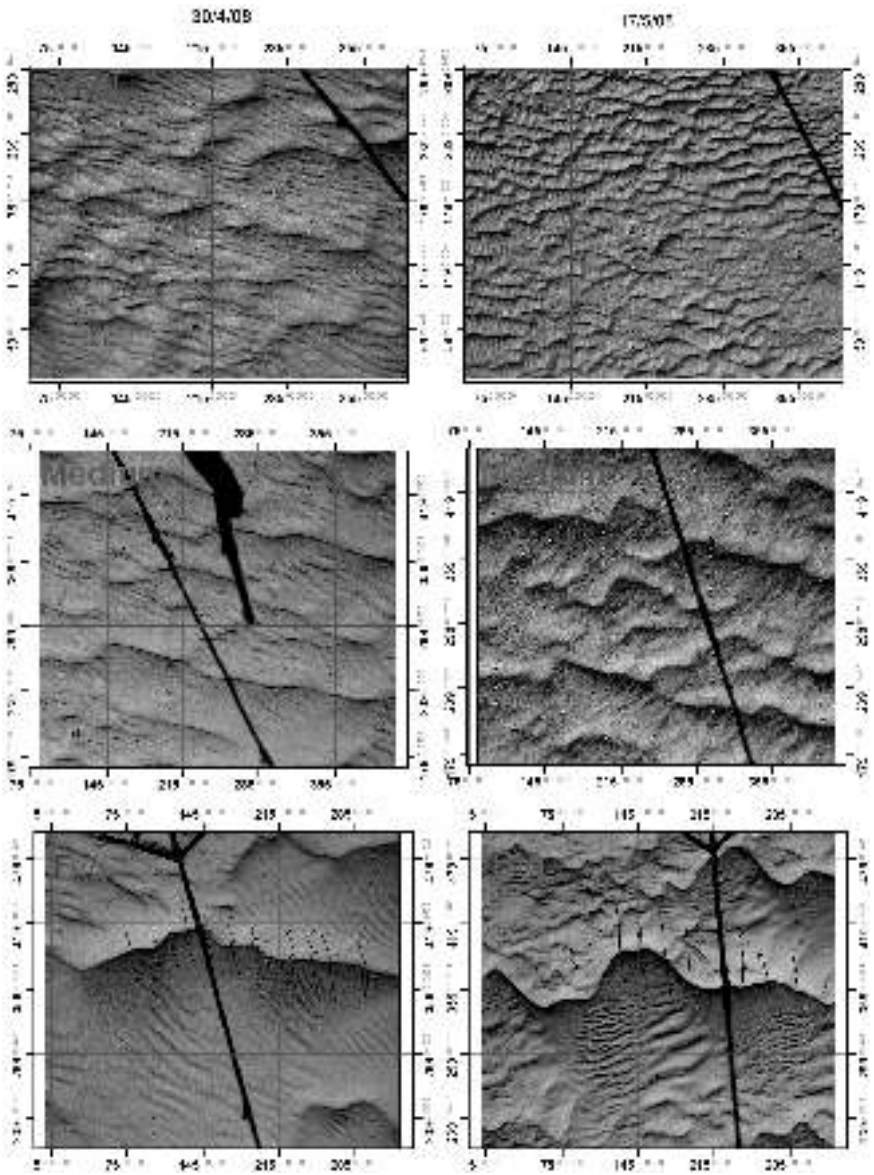

Fig. 16. Orthophotos of three plots before and after the storm of 8 May 2008. The wind direction is from top to bottom in all the figures. The names of the plots refer to the relative sizes of the mega-ripples (where Small refers to plot C, Medium to plot B, and Big to plot D). See text for details.

are characterized by mega-ripples of small ($\lambda = 50$ cm), medium ($\lambda = 73$ cm), and large ($\lambda = 120$ cm) wavelength. In the "small" plot, the storm's effect was dramatic. The mega-ripples were broken into small ripples ($\lambda =$ 15 cm) that cover the entire plot. This effect was probably caused by the strong wind that was above the fluid threshold of the coarse particles on the mega-ripple crests, in agreement with Bagnold's (1941) observation. In the "medium" plot, the mega-ripple wavelength remained nearly unchanged, although the mega-ripples drifted downwind and in some places the crests broke due to a nonuniform drift velocity along the crest-line. The "big" mega-ripple in the third plot also drifted downwind and its height increased. The sinuosity of the crest line increased as it developed two lobes that moved faster than the center part. On the lee slope of the mega-ripples, two sizes of ripples developed as a result of different fractions of coarse grains. This dependence of mega-ripple behavior on size suggests that on the bigger mega-ripples, the grains that armor the crests are coarser and cannot be entrained by normal wind strengths. They require extremely strong winds to bring about saltation. According to eq 5, a wind speed of 15 m/s is needed to entrain 1-mm grains.

Although the storm of 8 May 2008 reached such high speeds, these winds were short-lasting and during most of the storm the winds were commonly below the fluid threshold for the large grains on the major mega-ripple, but above the fluid threshold for coarse grains atop the small mega-ripples. Thus, there are critical mega-ripple sizes that determine different dynamics in response to storms. Large enough mega-ripples can continue to develop, while small mega-ripples can be destroyed. At the initial stage, mega-ripple development needs repeated exposure to moderate winds above 6 m/s and that blow in approximately the same direction. In Nahal Kasuy such winds occur during the summer. As the mega-ripple grows higher, it protrudes into zones of higher wind speed in the atmospheric boundary layer. The coarser crestal grains are more readily moved forward under the direct action of the wind (Thomas, 1997) and the mega-ripple can be flattened. This mechanism can set the upper limit for mega-ripple dimensions.

CONCLUSIONS

We present here the interim findings of an ongoing research in the mega-ripple field at Nahal Kasuy in the southern Negev. During the study period, the wind drift potential was low in its absolute value as well as relative to values in former years. Because of this low drift potential (DP), mega-ripples required more than a year to develop from a flat bed. Grain-size analyses from different parts of the mega-ripples and from normal ripples show that a bimodal mixture of grain sizes is needed for mega-ripple formation and that the coarse particles are more abundant at the crest. Photogrammetric analysis revealed that mega-ripples start out as normal ripples and grow due to a rapid coarsening process. Their evolution is a function of DP and the wind direction variability. The final wavelength is not simply correlated to the mean saltation length, but develops through interactions between ripples of different sizes. Larger wavelengths probably reflect longer development times and stronger winds. This is a common behavior of bedforms in different environments, such as ripples and dunes in rivers, oceans, and deserts (Werner, 1999). The mega-ripple system exhibits self-organization, where ordered spatio-temporal structures spontaneously emerge (Anderson, 1990; Werner, 1995; Kocurek and Ewing, 2005).

Storms can inject new defects into the system by breaking existing mega-ripple crests and changing their orientation. Our observation suggests that small mega-ripples can be broken into small ripples by strong winds ("coarse fraction impact ripples", according to Ellwood et al., 1975), whereas larger ones continue to grow. For mega-ripple evolution from a flat bed, more frequent moderate unidirectional winds accelerate the process. According to our results, the two important parameters that dictate mega-ripple spatio-temporal dynamics are DP and the grain-size distribution. Mega-ripples continue to grow as long as the wind speed is below the fluid threshold for the coarse grains on the crest.

A deeper understanding of the initial stage of mega-ripple formation can be gained by conducting wind tunnel experiments with different bimodal sand distributions and for different wind speeds. It will be particularly important to measure the minimal sorting index needed for mega-ripple formation and its dependence on the grain diameter ratio. Such controlled experiments will deepen our understanding of the complex nature of the interaction between wind and a mixture of grains sizes.

By applying the methods we developed in Nahal Kasuy to places with larger mega-ripples could help us verify our conclusions. The mega-ripples in Nahal Kasuy are small compared to those that were found in other sites, such as in Jordan or Brazil. The advantage of the Nahal Kasuy mega-ripples is that the timescale

of their development is approximately one year. It may take years for large mega-ripples to form even under a stronger wind environment. They are sensitive to wind action and their pattern can quickly change after strong storms that occur in the area in the winter and spring. However, it is clear that understanding the long-term development of huge mega-ripples ($\lambda = 18$ m), such as those in the Carachi Pampa, Argentina (Milana, 2009), can be effectively achieved only via mathematical modeling, which will include insights gained from field studies such as the one reported here.

ACKNOWLEDGMENTS

This work was supported by the Israel Science Foundation (grant N531/06). We thank Yosef Ashkenazy for providing the wind data of Uvda airport, Leonid Prigozhin for his comments, Roy Talbi for helping us with the wind measurements at Nahal Kasuy, and Roni Bluestein for the map preparations. We also thank the two reviewers, Douglas J. Jerolmack and Joanna E. Bullard, for their important comments.

REFERENCES

Anderson, R.S. 1990. Eolian ripples as example of self-organization in geomorphological systems. Earth-Science Reviews 29: 77–96.

Anderson, R.S., Haff, P.K. 1988. Simulation of eolian saltation. Science 241: 820–823.

Bagnold R.A. 1941. The physics of blown sand and desert dunes. Methuen, London.

Blott, S.J., Pye, K. 2001. GRADISTAT: A grain size distribution and statistics package for the analysis for unconsolidated sediments. Earth Surfaces and Landforms 26: 1237–1248.

Defoe, O.K., Compton, A.H. 1925. The density of rock salt and calcite. Physical Review 25(5): 618–620.

Edgett, K.S. 2001. Observations regarding small eolian dunes and large ripples on Mars. Geological Society of America Abstracts with Programs 33(6): 178–0.

Ellwood, J.M., Evans, P.D., Wilson, I.G. 1975. Small scale aeolian bedforms. Journal of Sedimentary Petrology 45: 554–561.

El-Baz, F., 1986. The formation and motion of dunes and sand seas. In: El-Baz, F., Hassan, M.H.A., eds. Physics of desertification. Martinus Nijhoff Publication, Dordrecht, pp. 78–79.

Fenton, J.D., Abbott, J.E. 1977. Initial movement of grains on a stream bed: the effect of relative protrusion. Proc. R. Soc. London 352-A: 523–537.

Fryberger, S.G., Hesp, P., Hastings, K. 1992. Aeolian granule deposits, Namibia. Sedimentology 39: 319–331.

Fryberger, S.G. 1979. Dune forms and wind regime. In: McKee, E.D., ed. A study of global sand seas. U.S. Geol. Surv. Prof. Pap. 1052, Washington, DC, pp. 137–169.

Greeley, R., Bridges, N.T., Kuzmin, R.O., Laity, J.E. 2002. Terrestrial analogs to wind-related features at the Viking and Pathfinder landing sites on Mars. Journal of Geophysical Research-Planets 107(E1): Art. no. 5005, 25 Jan 2002.

Ginat, H. 1991. The geology and geomorphology of Yotvata Region. M.Sc. thesis, Hebrew University, Jerusalem (in Hebrew, English summary).

Goldreich, Y. 1998. The climate of Israel. Observations, research and applications. Bar-Ilan Press, Ramat Gan.

Jerolmack, D.J., Mohrig, D., Grootzinger, J.P., Fike, D., Watters, W.A. 2006. Spatial grain size sorting in eolian ripples and estimation of wind conditions on planetary surfaces: application to Meridiani Planum, Mars. Journal of Geophysical Research-Planets 111(E5): Art. No. E12S02.

Kocurek, G., Ewing, R.C. 2005. Aeolian dune field self-organization implications for the simple versus complex dune-field patterns. Geomorphology 72: 94–105.

Kuragano, T., Yamaguchi, A. 2006. Curve shape modification and similarity evaluation. CIMCA, International Conference on Computational Intelligence for Modelling Control and Automation and International Conference on Intelligent Agents Web Technologies and International Commerce (CIMCA'06), p. 227.

Lee, J.A., Allen, B.L., Peterson, R.E., Gregory, J.M., Moffett, K.E. 1994. Environmental controls of blowing dust direction at Lubbock, Texas, USA. Earth Surface Processes and Landforms 19: 437–449.

Milana, J.P. 2009. Largest wind ripples on Earth? Geology 37: 343–346.

Mountney, N.G., Russell, A.J. 2004. Sedimentology of cold-climate Aeolian sandsheet deposits in the Askja region of northeast Iceland. Sedimentology 166: 223–244.

Murray, A.B. 2005. Bedform pattern evolution in two horizontal dimensions: extreme wavelength increases with mixed grain sizes. Geophysical Research Abstracts 7: 01859.

Raudkivi, A.J., Ettema, R. 1982. Stability of armour layers in rivers. Journal of the Hydraulics Division, American Society of Civil Engineers 108(HY9): 1047–1057.

Rubin, D.M. 2006. Ripple effect: unforeseen applications of sand studies. Eos 87: 30, 293, 297.

Sakamoto-Arnold, C.M. 1988. Eolian features produced by the December 1977 windstorm Southern San Joaquin Valley, California. Journal of Geology 89: 129–137.

Sharp, R.P. 1963. Wind ripples. Journal of Geology 71: 617–636.

Thomas, D.S.G. 1997. Sand seas and aeolian bedforms. In: Thomas, D.S.G., ed. Arid zone geomorphology. John Wiley, New York.

Tsoar, H. 1990. Grain-size characteristics of wind ripples

on a desert seif dune. Geography Research Forum 10: 37–50.

Walker, D.J. 1981. An experimental study of wind ripples. M.Sc. thesis. Massachusetts Institute of Technology, Cambridge, MA.

Werner, B.T. 1995. Eolian dunes. Computer simulations and attractor interpretation. Geology 23: 1107–1110.

Werner, B.T. 1999. Complexity in natural landform patterns. Science 24: 102–104.

Wiberg, P.L., Smith, J.D. 1987. Calculations of the critical shear stress for motion of uniform and heterogenous sediments. Water Resources Research 23(8): 1471–1480.

Wiggs, G.F.S. 1997. Sediment mobilization by the wind. In: Thomas, D.S.G., ed. Arid zone geomorphology. John Wiley, New York.

Williams, S.H., Zimbelman, J.R., Ward, A.W. 2002. Large ripples on earth and Mars. Lunar and Planetary Science XXXIII, 1508.pdf.

Wilson, S.A., Zimbelman, J.R., Williams, S.H. 2003. Large aeolian ripples: extrapolations from Earth to Mars. Lunar and Planetary Science XXXIV, 1862.pdf.

Yizhaq, H. 2005. A mathematical model for aeolian mega-ripples on Mars. Physica A 357: 57–63.

Yizhaq, H. 2008. Aeolian megaripples: mathematical model and numerical simulations. Journal of Coastal Research 24(6): 1369–1378.